Hindawi Publishing Corporation
Journal of Solar Energy
Volume 2014, Article ID 892348, 13 pages
http://dx.doi.org/10.1155/2014/892348

Research Article

Thermoeconomic Analysis and Multiobjective Optimization of a Solar Desalination Plant

Hamid Mokhtari, Mokhtar Bidi, and Mahdi Gholinejad

Faculty of Mechanical & Energy Engineering, Shahid Beheshti University, A.C., 1983963113 Tehran, Iran

Correspondence should be addressed to Mokhtar Bidi; m_bidi@sbu.ac.ir

Received 26 May 2014; Revised 17 August 2014; Accepted 18 August 2014; Published 16 September 2014

Academic Editor: Santanu Bandyopadhyay

A solar desalination plant consisting of solar parabolic collectors, steam generators, and MED unit was simulated technoeconomically and optimized using multiobjective genetic algorithm. A simulation code was developed using MATLAB language programming. Indirect steam generation using different thermal oils including THERMINOL VP1, THERMINOL66, and THERMINOL59 was also investigated. Objective function consisted of 17 essential parameters such as diameter of heat collector element, collector width, steam generator pinch, approach temperatures, and MED number of effects. Simulation results showed that THERMINOL VP1 had superior properties and produced more desalinated water than other heat transfer fluids. Performance of the plant was analyzed on four characteristic days of the year to show that multiobjective optimization technique can be used to obtain an optimized solution, in which the product flow rate increased, while total investment and O&M costs decreased compared to the base case.

1. Introduction

Limited sources of clean potable water have motivated humans to find alternative sources to resolve the problem. Industrial desalination plants are among the best technological solutions for clean water production from sea water. Traditional plants use fossil fuels to provide required steam but, nowadays, using solar collectors has become more attractive to prevent global pollution. For example, in the southwestern part of USA, in 2010, only about 1.0 Gm^3/year of water demand was provided by solar desalination technologies, while, in 2014, this portion reached 3.0 Gm^3/year, which shows 200% increase during 4 years. Prediction says that this value would be increased to 12.0 Gm^3/year by 2050 [1]. A list of installed desalination plants operated with renewable energy sources up to 2003 is given by Tzen and Morris [2]. Beside industrial development, many research groups have focused on developing software tools to simulate, investigate, and theoretically optimize desalination plants. For example, Kamali et al. [3] developed a code for thermal simulation of multieffect desalination-thermal vapor compression (MED-TVC) unit to find optimized parameters for higher gain output ratio (GOR). They concluded that thermal optimization could lead to higher GOR in a constant surface area for a sample of 1500 m^3/day unit. They also completed their codes to implement evaporator, thermocompressor, and ejector design and study Qeshm island MED unit [4]. Skiborowski et al. [5] used mixed integer nonlinear programming (MINLP) algorithm to optimize two reverse osmosis (RO) and MED desalination unit in combination with a thermal power plant.

Multiobjective optimization technique based on the genetic algorithm was proved to be a reliable tool for techno-economic improvement of plants and has been used by many researchers. Najafi et al. [6] utilized this technique for optimizing solid oxide fuel cell- (SOFC-) gas turbine hybrid cycle coupled with an MSF desalination unit. Exergy efficiency, total cost, and environmental pollutants were included in their objective function. The technique was used by Shahandeh et al. [7] to optimize a heat-integrated distillation column and was also applied by Janghorban Esfahani and Yoo [8] to enhance efficiency of a cogeneration plant. Ansari et al. [9] used the technique to minimize water and power production cost. In a similar study, Sayyaadi

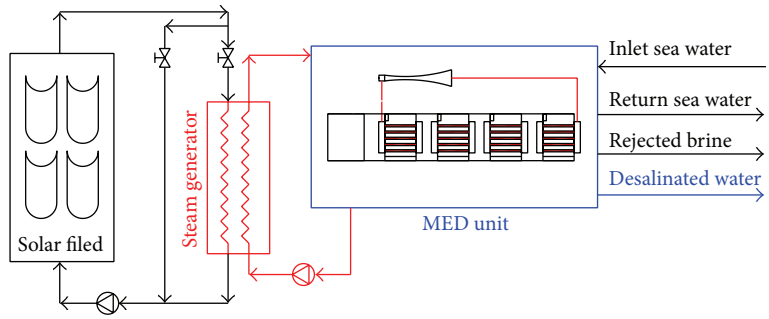

Figure 1: Schematic diagram of the solar desalination plant.

et al. [10] investigated the optimum parameters of an MED-TVC unit using a hybrid metaheuristic optimization tool. Khoshgoftar Manesh et al. [11] tried to find optimal coupling of MED-RO desalination plant using genetic algorithm and exergoeconomic optimization.

In the case of solar applications, there are some studies that use genetic algorithm to find optimal solutions, which include the study performed by Silva et al. [12] for optimizing a solar field with parabolic collectors.

It is important to note that there are various types of desalination technologies including [13]

(i) multistage flash (MSF),

(ii) multiple effect boiling (MEB) or multieffect desalination (MED),

(iii) vapor compression (VC),

(iv) freezing,

(v) humidification-dehumidification (HD),

(vi) solar stills,

(vii) membrane processes.

Industrial desalination technologies either use phase change or involve semipermeable membranes to separate the solvent or some solutes. Therefore, desalination techniques may be classified into the following categories: phase change or thermal processes and membrane or single-phase processes.

In the phase change or thermal processes, distillation of seawater is achieved by utilizing a thermal energy source. Thermal energy may be obtained from a conventional fossil fuel source, nuclear energy, nonconventional solar energy source, or geothermal energy. In the membrane processes, electricity is used for either driving high-pressure pumps or ionizing salts contained in the seawater.

Some researchers have focused on "humidification-dehumidification (HD)" technologies for solar desalination. For example, Kabeel and El-Said [14, 15] investigated a hybrid solar desalination system of air humidification, dehumidification, and water flashing evaporation by both numerical and experimental techniques. Chang et al. [16] studied the effect of sea water flow rate on the performance of a solar desalination plant using porous balls technique. Li et al. [17] built a small-scale humidification-dehumidification desalination unit to test the effect of various parameters on the unit performance. Their results showed that different inlet sprayed water temperatures in the pad humidifier from 9 to 27°C can effectively improve relative humidity of outlet moist air from 89 to 97% and the outlet air temperature from 35 to 42°C. Other researchers (e.g., [18–22]) have investigated HD technologies to produce potable water at small-scale units, which is applicable for small-scale users.

Some others have studied solar stills, for example, Ranjan and Kaushik [23] performed an energy and exergy analysis on a solar pool desalination plant.

However, commercial desalination processes based on thermal energy are multistage flash (MSF) distillation, multiple-effect desalination (MED), and vapor compression (VC), which could be thermal (TVC) or mechanical (MVC) vapor compression.

On the other hand, according to a survey conducted under a European research project [24], the most promising and applicable solar desalination technologies were MSF and MED. A list of installed desalination plants operated with renewable energy sources up to 2003 was presented by Tzen and Morris [2]. Hu and Chen [25] designed a small-scale solar multieffect desalination unit using parabolic collectors to evaporate the sea water.

At the present study, solar MED-TVC technology as the combination of multiple-effect desalination (MED) and thermal vapor compression (TVC) was investigated. The plant was designed for a moderate town with demand of 2000–5000 m^3/day. Multiobjective genetic algorithm optimization technique was used to find optimum parameters of a solar desalination plant, which is schematically shown in Figure 1. A heat transfer fluid (HTF) is heated and circulates in a closed system of parabolic collectors and transfers the absorbed solar energy to heating water in the steam generator. The produced steam is condensed at the first effect of the MED unit and causes the sea water to evaporate. The vapor is then condensed into desalinated water (product water) at the next effect by another sea water stream. The plant is located in the city of Ahwaz, in the southeastern part of Iran. The main objectives and contribution of this paper include the following items:

(i) multiobjective optimization of a solar desalination plant using genetic algorithm,

(ii) considering maximum water production and minimum costs as the multiobjective function for the optimization,

(iii) investigating the effect of different thermal oils on the plant efficiency and water production rates,

(iv) performance of solar desalination plant have been analyzed at four characteristics days of the year, including spring equinox, summer solstice, fall equinox, and winter solstice,

(v) sensitivity analysis on solar collector acceptance angle,

(vi) plotting Pareto curve, finding the optimum parameters, and comparing them with the design parameters,

(vii) exact calculation of radiative heat loss for the parabolic collector.

2. Mathematical Modeling

2.1. Solar Collector Heat Transfer Equations. Mathematical modeling of solar parabolic collectors has been performed by many researchers (e.g., [26, 27]). One-dimensional energy balance model developed by Tao and He [26] was adapted here. For short receivers (<100 m), a one-dimensional energy balance provides reasonable results; for longer receivers, a two-dimensional energy balance is necessary. The model determines the performance of a parabolic trough solar collector's linear receiver, also called a heat collector element (HCE). Inputs of the model include collector and HCE geometry, optical properties, heat transfer fluid (HTF) properties, HTF inlet temperature and flow rate, solar insulation, wind speed, and ambient temperature. Outputs include collector efficiency, outlet HTF temperature, heat gain, and heat and optical losses. Modeling assumptions and limitations were also discussed along with recommendations for model improvement.

Figure 2 shows the one-dimensional steady-state energy balance for a cross-section of an HCE without the glass envelope intact. The optical losses are due to imperfections in the collector mirrors, tracking errors, shading, and mirror and HCE cleanliness.

The effective incoming solar energy (solar energy minus optical losses) is absorbed by the absorber selective coating $\dot{q}'_{3\text{SolAbs}}$. Some energy that is absorbed into the selective coating is conducted through the absorber ($\dot{q}'_{23\text{cond}}$) and transferred to the HTF by convection ($\dot{q}'_{12\text{conv}}$); the remaining energy is transmitted back to (is lost) to the environment by convection ($\dot{q}'_{36\text{conv}}$) and radiation ($\dot{q}'_{37\text{rad}}$) and through the HCE support bracket through conduction ($\dot{q}'_{\text{cond, bracket}}$). The model assumes that all temperatures, heat fluxes, and thermodynamic properties are uniform around the circumference of the HCE. Also, all flux directions shown in Figure 2 are positive. Consider

$$\begin{aligned}
\dot{q}'_{12\text{conv}} &= \dot{q}'_{23\text{cond}} \\
\dot{q}'_{3\text{SolAbs}} &= \dot{q}'_{36\text{conv}} + \dot{q}'_{37\text{rad}} + \dot{q}'_{23\text{cond}} + \dot{q}'_{\text{cond, bracket}} \\
\dot{q}'_{\text{HeatLoss}} &= \dot{q}'_{36\text{conv}} + \dot{q}'_{37\text{rad}} + \dot{q}'_{\text{cond, bracket}}.
\end{aligned} \tag{1}$$

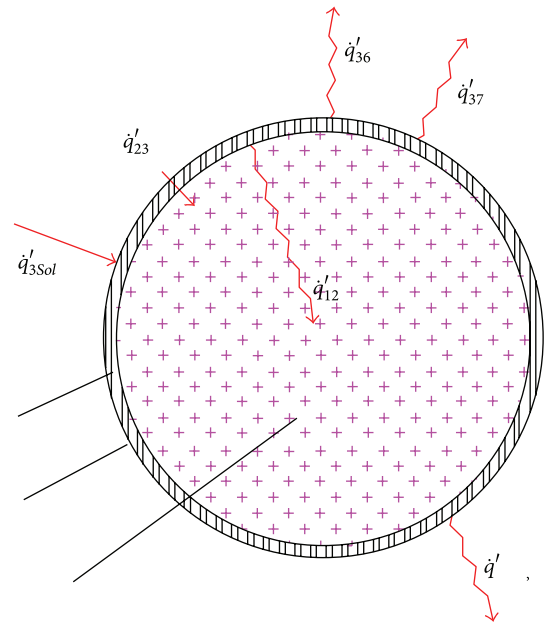

Figure 2: One-dimensional steady-state energy balance and for a cross-section of an HCE.

From Newton's law of cooling, the convection heat transfer from the inside surface of the absorber pipe to the HTF per unit length of the pipe is

$$\begin{aligned}
\dot{q}'_{12\text{conv}} &= h_{\text{HTF}} D_1 \pi \left(T_2 - T_1\right), \\
h_{\text{HTF}} &= \text{Nu}_{D2} \frac{k_1}{D_2}.
\end{aligned} \tag{2}$$

To model the convective heat transfer from the absorber to the HTF for turbulent and transitional cases (Reynolds number > 2300), the following Nusselt number correlation developed by Gnielinski [28] is used:

$$\begin{aligned}
\text{Nu}_{D2} &= \frac{(f/8)\left(\text{Re} - 1000\right)\text{Pr}_1}{1 + 12.7\sqrt{f/8}\left(\text{Pr}_1^{2/3} - 1\right)}\left(\frac{\text{Pr}_1}{\text{Pr}_2}\right)^{0.11}, \\
f &= \left[1.82\log_{10}\left(\text{Re}_{D2}\right) - 1.64\right]^{-2},
\end{aligned} \tag{3}$$

in which f is the friction factor for the inner surface of the absorber pipe and Pr_1 and Pr_2 are Prandtl number evaluated at the HTF temperature, T_1, and the inner surface temperature, T_2, respectively.

Fourier's law of conduction through a hollow cylinder describes the conduction heat transfer through the absorber wall [29]:

$$\dot{q}'_{23\text{cond}} = \frac{2\pi k\left(T_2 - T_1\right)}{\ln\left(D_1/D_2\right)}. \tag{4}$$

The conduction coefficient depends on the absorber material type. In this research, the HCE performance model includes three stainless steels, 304L, 316L, and 321H, and one copper.

If there is a wind, the convection heat transfer from the glass envelope to the environment will be forced convection. The Nusselt number in this case is estimated with

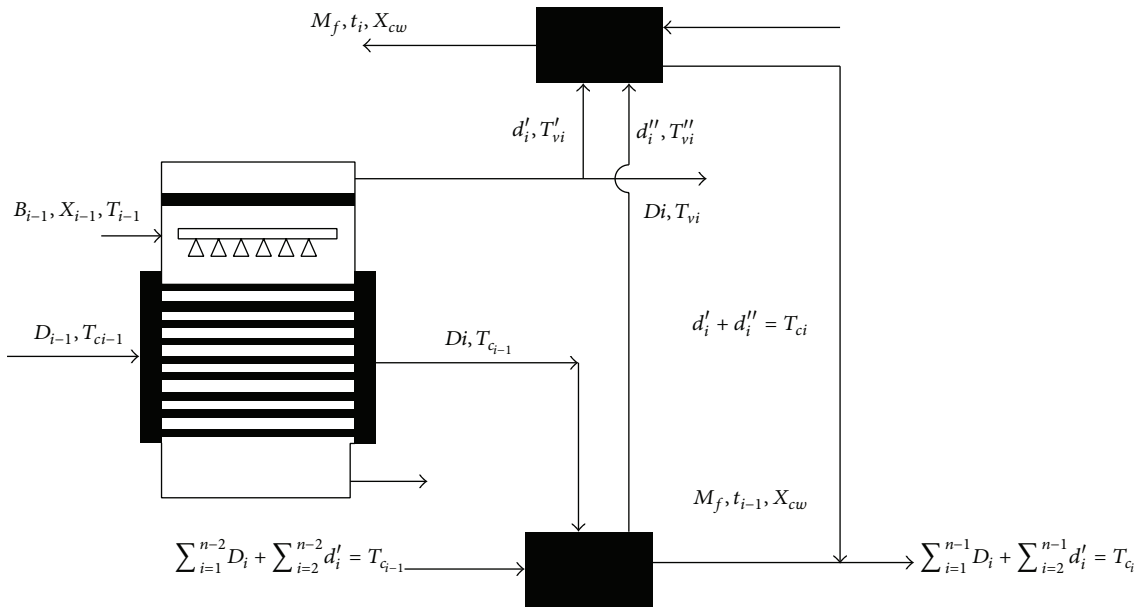

Figure 3: Heat and mass balance diagram for ith effect [33].

Zhukauskas' correlation for external forced convection flow normal to an isothermal cylinder [29]:

$$\mathrm{Nu}_{D3} = \mathrm{CRe}_{D_3}^{m} \mathrm{Pr}_4^{n} \left(\frac{\mathrm{Pr}_4}{\mathrm{Pr}_3} \right)^{1/4}. \tag{5}$$

The net radiation transfer between the absorber pipe and sky becomes [29]

$$\begin{aligned} \dot{q}'_{37\mathrm{rad}} &= A_1 F_{\mathrm{sur}} \left(J_1 - J_{\mathrm{sur}} \right), \\ J_1 &= E_{b1} - q \frac{(1-\varepsilon_1)}{\varepsilon_1 \pi D}, \\ J_{\mathrm{sur}} &= \sigma T_{\mathrm{Sky}}^4, \\ F_{\mathrm{sur}} &= \frac{\theta}{360}, \end{aligned} \tag{6}$$

in which σ is the Stefan-Boltzmann constant, ε is the emissivity of the pipe outer surface, D is the pipe outside diameter, and θ is the collector angle with the sky. Sky temperature, T_{sky}, is calculated using Ouagued et al. [30] correlation.

Other terms in (1) can be calculated using models and equations of other references (e.g., [31, 32]) and are not mentioned here to prevent elongation of the paper.

2.2. MED Design Model and Equations. An MED unit includes multiple effects which are similar to each other in terms of energy and mass balance. Figure 3 shows a schematic balance diagram for ith effect [33]. To simulate the MED process, it is necessary to solve equations of water mass balance, salt mass balance, and energy balance in each single effect and in the MED unit overall.

Water Mass Balance

Consider

$$F_i + B_{i-1} = D_i + B_i, \tag{7}$$

where F, B, and D are feed water flow rate, brine flow rate, and desalinated water flow rate, respectively, and i is the ith effect no.

Salt Mass Balance

Consider

$$F_i X_{F_i} + X_{B_{i-1}} B_{i-1} = X_{B_i} B_i, \tag{8}$$

where X_B is the outlet brine concentration (in ppm) with the maximum of 70000 ppm [33].

Energy Balance Equation

Consider

$$D_{i-1}\lambda_{i-1} + d_{i-1}\lambda_{i-1} + d'_{i-1}\lambda'_{i-1} = F_i C_p \left(T_i - T_f \right) + D_i \lambda_i, \tag{9}$$

where λ_i is the latent heat of vaporization in ith effect, d_{i-1} is the amount of vapor formed by brine flashing in effect $i-1$, and d'_{i-1} is the amount of vapor formed by flashing in the flashing boxes.

The main objective of MED simulation is to calculate desalinated water flow rates D_i and d'_i in each effect and then summarize them to calculate total desalinated water. To do this, a detail physical and mathematical modeling of heat transfer inside and outside the tubes in each effect and also in condenser and thermocompressor is required. The mathematical modeling of El-Dessouky et al. [33] is adapted here and is ignored for abbreviation.

The formula presented by Han and Fletcher [34] is used in this model for evaluation of the falling film evaporation heat transfer coefficient over horizontal tubes:

$$h_o\left(\frac{\mu_{sw}^2}{\rho_{sw}^2 g k_{sw}^3}\right)^{1/3} = 0.0004\mathrm{Re}^{0.2}\mathrm{Pr}^{0.65}\left(q''\right)^{0.4}, \quad (10)$$

where

$$\mathrm{Re} = \frac{4\times \dot{M}_f}{2\times \mu_{sw} L_{\mathrm{effect}}\sqrt{N}}. \quad (11)$$

For condensation inside the tubes of the effects, the formula presented by Xu et al. [35] is used:

$$\overline{h}_i = k^+\left(\frac{g\rho_L\left(\rho_L-\rho_v\right)k_L^3 h'_{fg}}{\mu_L d_i\left(T_{\mathrm{sat}}-T_{\mathrm{wall,in}}\right)}\right)^{1/4}, \quad (12)$$

where

$$k^+ = 0.3508\left(\frac{L}{d_i}\right)^{-0.1929}\cdot \mathrm{Re}^{0.0643},$$
$$\mathrm{Re} = \frac{d_i V_v \rho_L}{\mu_L}. \quad (13)$$

Heat transfer coefficients inside and outside of the condensers tubes are calculated using equations given by Wangnick [36]:

$$h_{ic} = \left(3293.5 + T\left(84.24 - 0.1714T\right)\right.$$
$$\left.-X\left(8.471 + 0.1161X + 0.2716T\right)\right)$$
$$\times\left(\left(\frac{d_{ic}}{0.17272}\right)^{0.2}(0.656V)^{0.8}\left(\frac{d_{ic}}{d_{oc}}\right)\right)^{-1}, \quad (14)$$

$$h_{oc} = 0.728\left(\frac{g\rho_L\left(\rho_L-\rho_v\right)k_L^3 h'_{fg}}{N_c\mu_L d_{oc}\left(T_{\mathrm{sat}}-T_{\mathrm{wall,out}}\right)}\right)^{1/4},$$

where

$$h'_{fg} = h_{fg} + \frac{3}{8}C_{p,l}\left(T_{vi}-T_{\mathrm{wall,in}}\right). \quad (15)$$

3. Economic Analysis

Total capital investment (TCI) is the sum of fixed capital investment (FCI) and other outlays including start-up cost (SUC), working cost (WC), cost of licensing, research, development (LRD), and allowance for funds used during construction (AFUDC) [37, 38].

In addition to equipment case, other installation costs like piping should be considered. The cost for piping includes the material and labor costs of all items required to complete the erection of all the piping used directly in the system. This cost represents 10–70% of the purchased-equipment cost. The following relation can be supposed to calculate piping cost [38]:

$$\mathrm{TCI} = \mathrm{FCI} + \mathrm{SUC} + \mathrm{WC} + \mathrm{LRD} + \mathrm{AFUDC}. \quad (16)$$

In addition to equipment case, other installation costs like piping should be considered. The cost for piping includes the material and labor costs of all items required to complete the erection of all the piping used directly in the system. This cost represents 10–70% of the purchased-equipment cost. The following relation can be supposed to calculate piping cost [38]:

$$Z_{\mathrm{pipe}} = \mathrm{PEC}_w\left(\frac{X_y}{X_w}\right)^{\alpha}. \quad (17)$$

Using this equation, pipe cost can be estimated for a desired diameter X_y knowing pipe cost for a specific pipe diameter X_w. In the above equation, X_y is greater than X_w and power factor α is usually less than unity and can be considered as 0.95.

Collector cost estimation was performed using correlations in [31]. For other pieces of equipment including MED, solar collectors, and steam generator, the cost estimation formulas used in [28–31] were ignored here for shortening.

Considering plant lifetime, n, and interest rate, i, capital recovery factor (CRF) was calculated by

$$\mathrm{CRF} = \frac{i(1+i)^n}{(1+i)^n - 1}. \quad (18)$$

Knowing all equipment, piping, and onsite costs, total cost investment (TCI) could be calculated. Then, cost of produced water per unit of mass flow rate was calculated using the following equation:

$$\dot{C}_{\mathrm{Cost}} = \frac{\mathrm{TCI}}{\dot{m}_{\mathrm{des}}}. \quad (19)$$

There are different methods to express total investment cost as a function of designed parameters. The method used in this paper is based on calculation of total cost per unit of time [39]:

$$\dot{Z}_K = \frac{\mathrm{TCI}\times \mathrm{CRF}\times \varphi}{N\times 3600}, \quad (20)$$

in which K represents the equipment, component, or system, N is number of operational hours per year, and φ is the operation and maintenance (O&M) coefficient which is selected as 1.06 (according to [40, 41]).

4. Objective Function

Maximum desalinated water production rates as well as minimum total capital investment were the main items of the objective function in the present study. Thus, the objective function could be formulated by a combination of desalinated water mass flow rate and desalinated water cost:

$$\dot{C}_{\mathrm{Cost}} = \sum\left(\mathrm{TCI}\right), \quad (21)$$

$$\dot{m}_{\mathrm{des}} = \sum_{i=1}^{n}\left(D_i + d_i\right). \quad (22)$$

Table 1: Lower and upper bounds of decision variables.

Decision variable	Lower bound	Upper bound
T_{pp} (°C)	5	50
T_{ap} (°C)	5	50
$d_{i,e}$ (mm)	20	80
H_C (m)	1	5
L_{co} (m)	1	5
W_C (m)	1	5
No. effect (—)	3	10
L_e (m)	1	8
$N_{t,c}$	10	50
$N_{t,e}$	10	50
$d_{o,c}$ (mm)	20	80
P (bar)	8	15
T_{sH} (°C)	200	400
D_2 (mm)	20	80
Thickness (mm)	10	25
$W_{Collector}$ (m)	3.5	8
V_{pipe}	1	3.5

As mentioned in Table 1, 17 variables, including thermodynamic and geometric parameters for steam generator, MED, and solar field, were considered the decision variables. Although the decision variables might vary in the optimization procedure, each was normally required to be within a reasonable range. The upper and lower bands of these parameters were selected based on the previous studies [8, 39, 42, 43].

5. Validation of Calculations and Results

5.1. Solar Collector Validation. Validation of the developed code was proved by comparison of the obtained results with the reported data of Dudley et al. [31], as shown in Figure 4. In this figure, thermal efficiency of the collector as a function of HTF average temperature is compared with the measured data and the maximum of 5% discrepancy is investigated. The model well predicted the collector behavior; that is, by increasing HTF temperature, heat losses increased, which in turn led to decrease in the collector thermal efficiency.

5.2. MED Design Validation. To validate the code, the simulation results for a MED unit including 7 effects were compared with the operational data of Kamali and Mohebinia [4]. Table 2 indicates the essential parameters of the unit and a comparison between the simulated results and reported data. As is shown, in the case of desalinated water flow rate, there was only 1.35% discrepancy between the measured data and simulated results.

6. Results and Discussions

6.1. Assumptions. Mathematical models were used for a desalination plant located in city of Ahwaz in the southeastern part of Iran. Table 3 shows the environmental conditions and constant parameters used in this simulation.

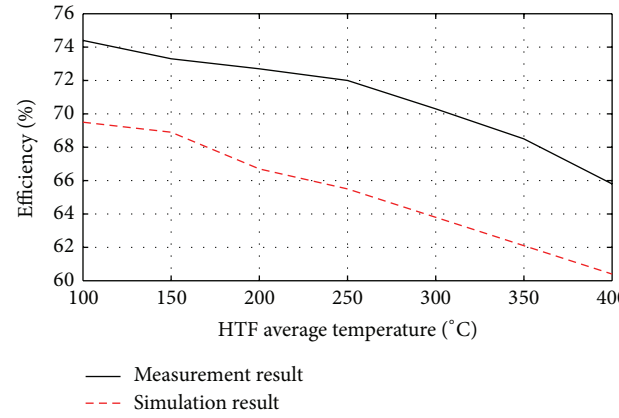

Figure 4: Effect of HTF average temperature on collector efficiency in compaction with measured data of Dudley et al. [31].

Properties of different thermal oils are mentioned in the Appendix. It is important to note that there is a higher limit of temperature for different oils to prevent oxidation. These limits are also presented in the Appendix. These temperature limits would affect the maximum collector pipe length, as will be discussed in the following sections.

6.2. Solar Field Simulation Results. To reach proper accuracy, total pipe length was divided into 4000 small distances. As the first comparison criterion, different maximum temperature limits were considered for different oils (according to the Appendix); therefore, different pipe lengths were considered for different oils, as shown in Table 4. Pipe pressure drop versus pipe segment is represented in Figure 5. From the beginning of the pipe up to 1000 segments, oil density and viscosity are decreased because of temperature rise; therefore, pressure drop is decreased. Since the mass flow rate is constant, after about 1500 segments, decreasing density leads to increase in volume flow rate and HTF velocity. This effect overcomes the viscosity effect and increases pressure drop. It is important to note that THERMINOL 66 has minimum pressure drop among different oils. However, to minimize the operational cost, the intention is to find the HTF with minimum pumping power.

Total pumping power is calculated from the following equation:

$$\dot{W}_p = \frac{\dot{m} \sum_{eleman=1}^{4000} \left(\Delta P(\text{bar}/m)_{eleman} \times L_{eleman}\right)}{\eta_p \rho} \quad (23)$$

in which L, ΔP, η_p, and ρ are element length, element pressure drop, pump efficiency, and oil density, respectively.

Therefore pumping power is proportional to both pressure drop and total pipe length. As seen from Figure 5, THERMINOL 66 has the minimum pressure drop in one pipe segment. If a unique total pipe length was considered for all oils, THERMINOL 66 would have the minimum pumping power. But in this research the considered limit for maximum allowable temperature led to different pipe length for different oils. Since THERMINOL 59 has the minimum pipe length

Table 2: Data validation for MED simulation.

Parameter	Unit	Operational data [4]	Simulated results	Difference (%)
Number of effects	—	7	7	Assumption
Length of tubes	M	4.1	4.1	Assumption
Motive steam pressure	Barg	10	10	Assumption
Motive steam temperature	°C	170	170	Assumption
Motive steam mass flow rate	tons/h	8	8	Assumption
Number of tubes in each effect	—	1996	1973	–1.17
Sea water flow rate	tons/h	420	429	2.10
Desalinated water flow rate (tons/d)	tons/d	1536	1557	1.35

Table 3: Environmental conditions and constant parameters for simulation.

Constant Parameter	Unit	Value
Latitude	°	31.30
Elevation from sea level	m	17.00
Average relative humidity	%	60.00
Average ambient temperature	°C	15.00
Mirror's Clearness efficiency	%	0.94
Reflection efficiency	%	0.93
Solar absorber pipe inside diameter	mm	65.00
Solar absorber pipe outside diameter	mm	75.00
Pipe material	—	steel 321H
Collector width	m	5.76
Collector acceptance angle	°	135

Table 4: Comparison of solar field parameters for different thermal oils considering maximum temperature limit for different oils.

	VP1	THERMINOL 66	THERMINOL 59
Length (m)	2455.50	1381.00	1107.50
T_{out} (°C)	399.02	344.04	314.04
W_{pump} (KW)	45.60	23.15	18.97
Dp_{Total} (bar)	46.55	24.27	19.46

(Table 4), therefore it has the minimum pumping power among the different oils.

Considering both pipe length and pressure drop, from data of Table 4, it can be concluded that pumping power is minimum for THERMINOL 59, while THERMINOL VP1 has maximum outlet temperature, maximum pipe length (maximum pipe cost), and maximum pumping power (maximum pump cost). On the other hand, this oil could produce more live steam which in turn causes production of more desalinated water and could be verified by Figure 6 that indicates the mass flow rate of desalinated water during the autumnal equinox. It can be concluded that, at the solar noon, water production rate for THERMINOL VP1 is 7.1% more than that for THERMINOL 59.

As the second comparison criterion, outlet temperature was considered 314°C for all oils which corresponded to the maximum acceptable temperature of THERMINOL 59. With this assumption, simulation results are summarized in

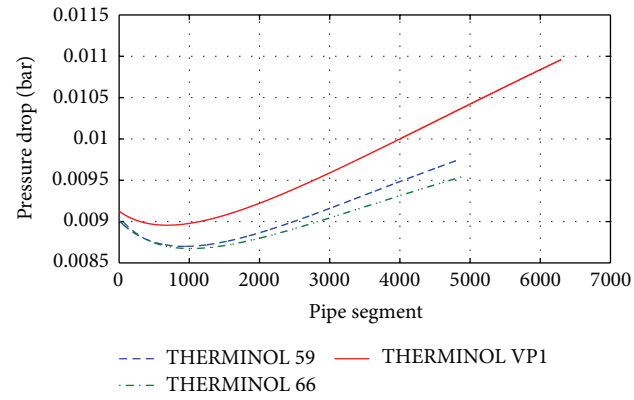

Figure 5: Pressure drop versus pipe segments for different thermal oils.

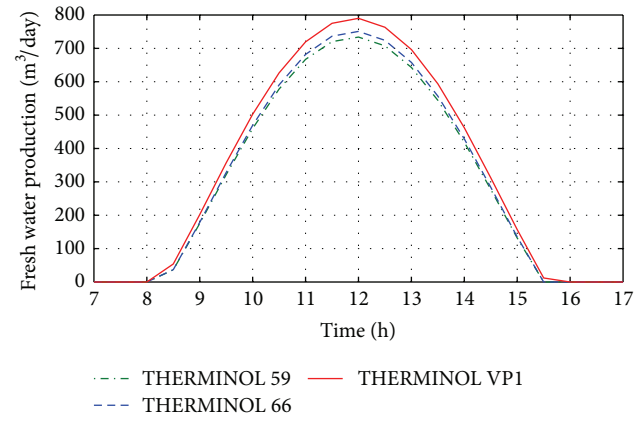

Figure 6: Variation of fresh desalinated water flow rate during the autumnal equinox for different thermal oils.

Table 5. In this case, THERMINOL 66 has minimum pipe length and minimum pumping power.

Bracket radiative and convective heat losses at the pipe inlet and outlet are indicated in Figure 7 for different oils. In the pipe inlet section, the surface temperature is low; therefore, the convective heat loss is more important than the radiative one. In contrast, in pipe outlet section, surface temperature is higher; therefore, the radiative heat loss becomes dominant. It can be verified from Figure 8 that, going through

Table 5: Comparison of solar field parameters for different thermal oils considering outlet temperature of 315°C for all the oils.

	VP1	THERMINOL 66	THERMINOL 59
Length (m)	1255	1107.0	1107.50
T_{out} (°C)	314.00	314.00	314.04
W_{pump} (KW)	21.81	18.49	18.97
Dp_{Total} (bar)	22.27	19.38	19.46

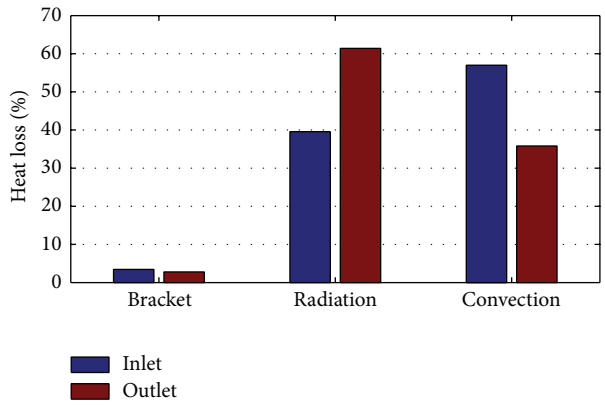

Figure 7: Heat loss mechanism at inlet and outlet of the collector pipe.

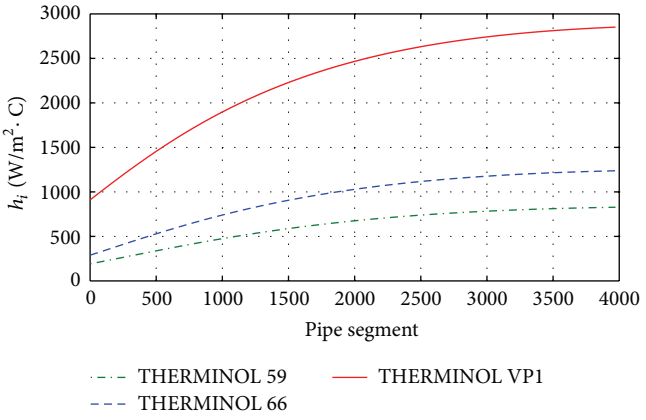

Figure 8: Inside heat transfer coefficient versus pipe segment for different thermal oils.

the pipe inlet to the pipe outlet segments, inside convective heat transfer coefficient increases; therefore, pipe surface temperature would be closer to the HTF higher temperature.

Sum of heat losses during pipe segments is shown in Figure 9 for different oils. THERMINOL VP1 has maximum heat loss compared to others.

Since the intention is to gain maximum solar energy, it is a good idea to use the oil with maximum temperature limit: THERMINOL VP1. Although it involves the greatest heat losses and maximum pumping power, its performance in producing higher desalinated flow rates is more attractive in technical and economic terms. Therefore, this oil was selected for the rest of calculations.

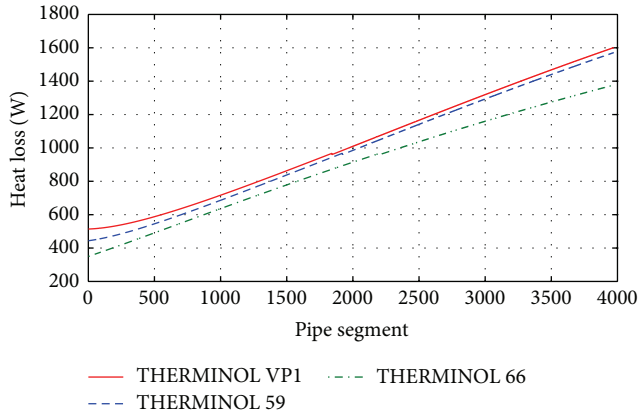

Figure 9: Total heat loss versus pipe segments for different thermal oils.

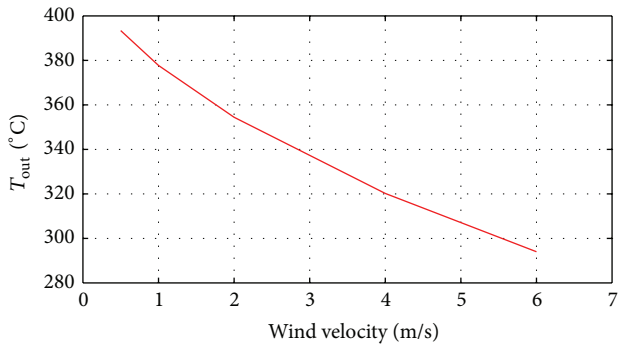

Figure 10: Variation of outlet HTF (selected THERMINO VP1) temperature versus wind velocity.

Figure 10 shows THERMINO VP1 outlet temperature as a function of wind velocity. It is clear that, with increasing wind velocity, convective heat losses increase and the outlet temperature decreases, which in turn leads to decreasing steam and water production rates. Therefore, it is recommended to use glass covers to reduce convective losses. If glass covers were used, energy balance equations would be slightly different from those established here.

6.3. MED Simulation Results. It is a general rule for MED units that, up to a specific limit, using more number of effects which means more heat transfer areas and more capital costs leads to producing more desalinated water with the same steam flow rate. This comment is verified by Figure 11.

6.4. Optimization by Multi Objective Genetic Algorithm. As stated previously, the intention was to optimize the solar MED plant using genetic algorithm (GA) with 17 decision variables (Table 1). The main objective function was to maximize desalinated water flow rate and minimize total capital investments (recall (20) and (21)). For simulating the plant, a MATLAB code was developed and, for its optimization, the multiobjective GA toolbox of this software was established. Prior to finding the optimized state of the plant, the decision

Table 6: Values of decision variables for the design and optimized case.

Decision variable	Design case value	Optimized case value
T_{pp} (°C)	20	9.41
T_{ap} (°C)	20	11.14
$d_{i,e}$ (mm)	28.75	48.17
H_C (m)	1	2.57
L_{co} (m)	3	2.31
W_C (m)	4.2	3.16
No. effect (—)	4	10.00
L_e (m)	4.1	2.42
$N_{t,c}$	16	23.39
$N_{t,e}$	35	29.00
$d_{o,c}$ (mm)	20	56.08
P (bar)	9	8.49
T_{sH} (°C)	200	210.37
D_2 (mm)	65	57.07
Thickness (mm)	15	14.21
$W_{Collector}$ (m)	5.76	7.53
V_{pipe}	2	3.21

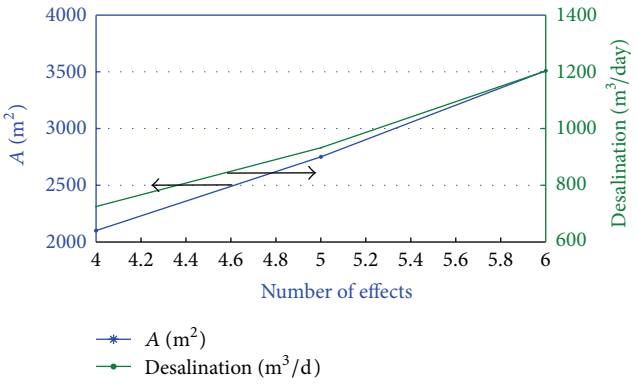

Figure 11: Variation of heat transfer area and desalinated water flow rate versus number of effects.

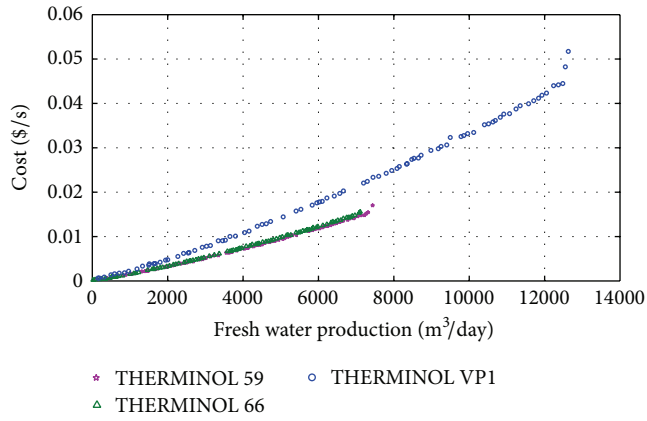

Figure 12: Pareto curves for different HTFs with objective function of water production and total capital investment.

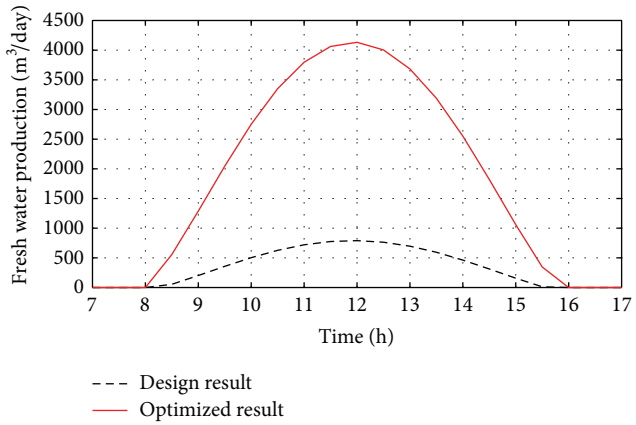

Figure 13: Comparison between design and optimized case in terms of fresh water production during spring equinox.

variables for THERMINOL VP1 were considered (according to Table 6) the base case (design case).

The optimization results are shown in Figure 12, as three Pareto curves for the three oils. According to this figure, THERMINOL VP1 shows a better behavior in terms of the specified objective function (minimize cost versus water production rate).

Using these Pareto curves, the absolute optimum point of the operation can be determined. In this case, a special code was used to determine the optimum point. Values of decision parameters for optimized case are presented in Table 6 for THERMINOL VP1. Comparison of these values with the original values of design case mentioned in Table 6 shows how this optimization differs from the base case.

To better understand the differences between the optimized case and the base case, four characteristic days of the year (i.e., spring equinox, summer solstice, fall equinox, and the winter solstice) were studied. Rates of solar flux on a horizontal surface for these characteristic days were 1010, 1200, 820, and 680 W/m^2, respectively. Figures 13, 14, 15, and 16 show that as solar flux decreases rate of the produced water also decreases but, there is a sensible difference between the base case and optimized case on all characteristic days.

For further analysis, both the design case and optimized case are compared in Figures 17 and 18 in terms of fresh desalinated water flow rate and total capital investment during autumnal equinox. As can be concluded from Figure 17, there is a considerable difference in water production rate between the two cases, especially at solar noon. On the other hand, total investment cost per cubic meter of produced water is also less in the optimized case, according to Figure 18. It is important to note that, during morning hours, oil temperature is less than the minimum desired value for steam generation; therefore, oil is bypassed from the steam generator and MED unit and circulated in a close loop of solar field. During this period of time, pumping costs are considered O&M costs.

Therefore, it can be concluded that the genetic algorithm is a powerful tool for optimization of a solar desalination plant in terms of technical and economical items.

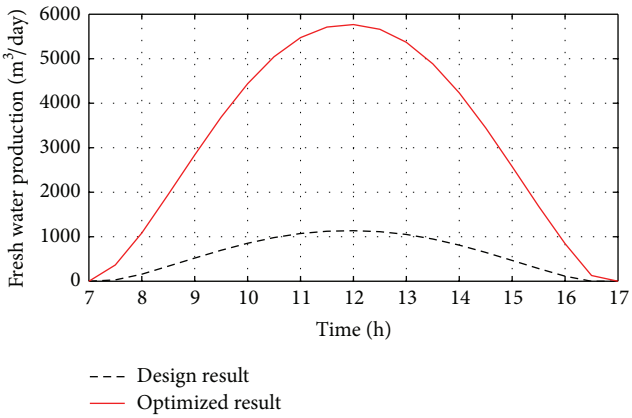

FIGURE 14: Comparison between design and optimized case in terms of fresh water production during summer solstice.

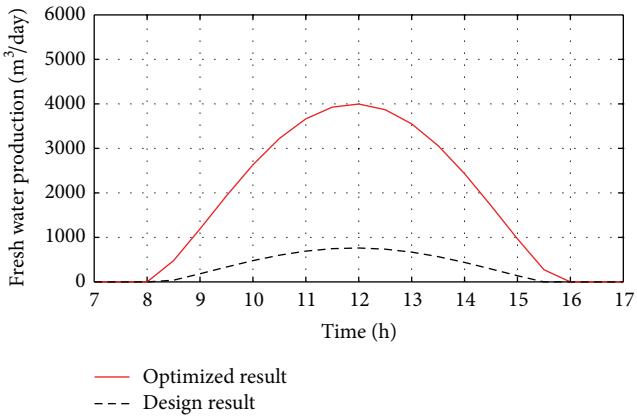

FIGURE 15: Comparison between design and optimized case in terms of fresh water production during autumnal equinox.

6.5. Sensitivity Analysis. To perform a sensitivity analysis, solar collector acceptance angle was reduced from 135 (design case) to 125 degrees and Pareto curves of both cases are plotted in Figure 18. It can be seen that, for a definite cost value of 0.0153 \$/s, the daily water production in the acceptance angle of 135 degrees is 352 cubic meters more than the case with 125 degrees of acceptance angle, while this difference decreases to 1.7 cubic meters per day for the cost of 0.005 \$/s.

Decreasing the collector acceptance angle from 135 to 125 degrees leads to considerable increase in cost. A slight variation in solar field parameters indicates that genetic algorithm changes the MED and steam generator design parameters simultaneously to reach the new optimized case.

7. Conclusion

The simulation results showed that, among three different thermal oils, THERMINOL VP1 needed greater pipe length than others considering the same outlet HTF temperature and produced more desalinated water, while total capital investments were of the same order.

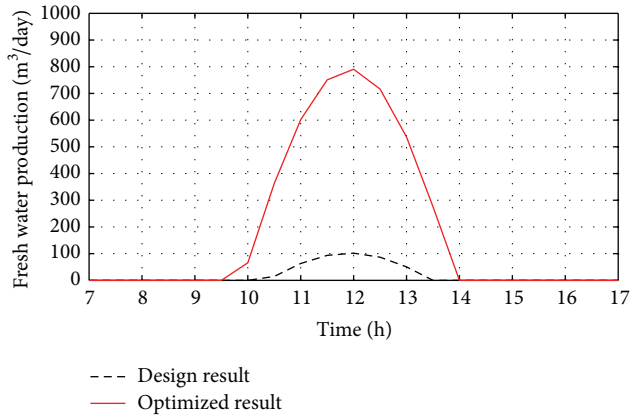

FIGURE 16: Comparison between the design and the optimized case in terms of fresh water production winter solstice.

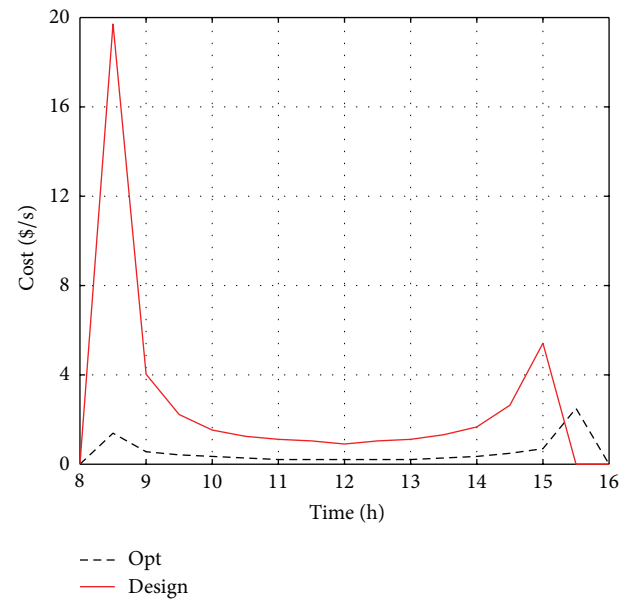

FIGURE 17: Comparison between design and optimized case in terms of cost of one cubic meter of produced fresh water during autumnal equinox.

Increasing wind velocity considerably decreased solar filed efficiency. On the other hand, increasing wind velocity from 0.5 to 2.0 m/s led to 10% increase in heat losses.

Using genetic algorithm for the plant optimization resulted in determining an optimized case which produced more desalinated water; meanwhile, its total investment cost was reduced. Pareto curves also indicated that THERMINOL VP1 had less price and higher water flow rates than other oils, which showed that GA well predicted the proper oil as was expected from the previous analysis and knowledge.

Reduction of solar collector acceptance angle from 135 to 125 degrees caused increasing the total cost in high water flow rates, while there was a small effect at low flow rates, indicating that GA led to change in design parameters of the

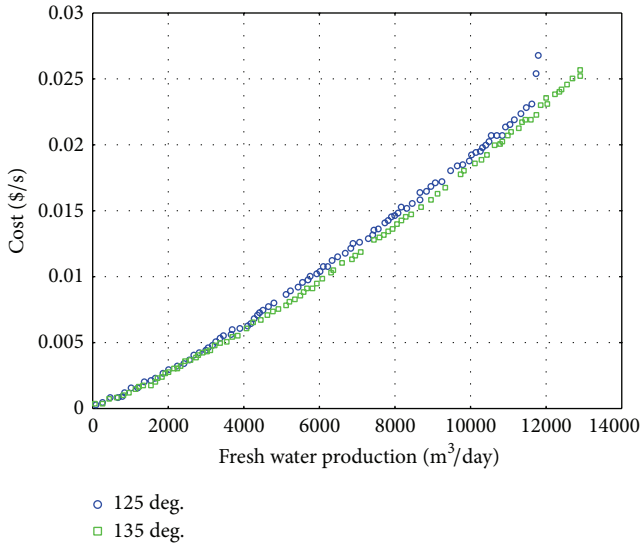

FIGURE 18: Sensitivity analysis on solar collector acceptance angle.

MED unit and steam generator as well as those of solar field simultaneously in order to determine the optimized case.

Appendix

Thermal Oil Properties

Property Equations for Various Thermal Oils. (see [44].)

THERMINOL VP1

Consider

$$\rho = -0.90T + 0.00078T^2 - 2.36 \times 10^{-6}T^3 + 1083.25$$

$$K = -8.19 \times 10^{-6}T - 1.92 \times 10^{-7}T^2 + 2.5 \times 10^{-11}T^3 - 7.29 \times 10^{-15}T^4 + 0.178$$

$$\mu = 0.1794 \times T^{-1.167}$$

$$C_p = 0.0024T + 5.95 \times 10^{-6}T^2 - 2.98 \times 10^{-9}T^3 + 4.41 \times 10^{-11}T^4 + 1.5$$

$$T_{\max}\,(^\circ\mathrm{C}) = 400. \tag{A.1}$$

THERMINOL 66

Consider

$$\rho = -0.614T - 0.00032T^2 + 1020.62$$

$$K = -3.3 \times 10^{-4}T - 1.5 \times 10^{-7}T^2 + 0.118294$$

$$\mu = 10^{-6} \times \rho \exp\left(\frac{386.375}{T + 62.5} - 2.2809\right)$$

$$C_p = 0.0033T + 8.9 \times 10^{-7}T^2 + 1.49$$

$$T_{\max}\,(^\circ\mathrm{C}) = 345. \tag{A.2}$$

THERMINOL 59

Consider

$$\rho = -0.692T - 0.0030T^2 + 1989.06$$

$$K = -6.4 \times 10^{-5}T - 1.3 \times 10^{-7}T^2 + 0.1226$$

$$\mu = 10^{-6} \times \rho \exp\left(\frac{503.471}{T + 100} - 2.25076\right) \tag{A.3}$$

$$C_p = 0.0031T + 5.4 \times 10^{-7}T^2 + 1.61$$

$$T_{\max}\,(^\circ\mathrm{C}) = 315.$$

Nomenclature

B: Parameter for estimation of BPE (°C)
C: Parameter for estimation of BPE (°C)
C_p: Heat capacity (kj/kg·K)
BPE: Boiling point elevation (°C)
D_2: Inlet diameter tube of absorber
$D_{i,e}$: Inlet diameter tube of effect
$D_{i,c}$: Inlet diameter tube of condenser
dT: Effects temperature difference (°C)
G: Mass flux, kg/(m^2·s)
g: Gravitational constant, 9.81 m/s^2
H_c: Height of condenser Shell
K_m: Heat transfer coefficient of tube wall (KW/kg°C)
L: Tube length (m)
L_e: Evaporator length (m)
$N_{t,e}$: Number of tubes on one line for effect
$N_{t,c}$: Number of tubes on one line for condenser
N_w: Number of rows wide
N_r: Number of tubes rows deep
Nu: Nusselt number
P.P: Pinch point (C or K)
P_{main}: Maine steam pressure
Re: Reynolds number
t: Tube of absorber thickness (mm)
V: Velocity (m/s)
v_f: Specific volume of fluid (m^3/kg)
W_c: Width of condenser Shell
$\dot{Z}$: Capital cost rate ($/s)
Z_K: Component purchase cost ($)

Greek Symbols

γ: Specific heat ratio
ρ: Density (kg/m^3)
ϕ: Maintenance factor
μ: Dynamic viscosity, kg/(s·m)
σ: Surface tension, kg/s^2

Subscripts

1: Heat transfer fluid
2: Inner absorber pipe surface
3: Outer absorber pipe surface
4: Ambient
5: Sky
B: Brine
Con: Condenser
Cond: Conduction
Conv: Convection
CRF: Capital recovery factor
Eva: Evaporation
F: Feed seawater
O: Out
I: Interest rate
In: Inlet condition
K: Component
P: Tube pinch (mm)
Sat: Saturated conditions
SH: Steam high pressure
SW: Seawater
V: Vapor phase.

Conflict of Interests

The authors declare that there is no conflict of interests regarding the publication of this paper.

References

[1] M. Stroud, *Solar Desalination in the Southwest United States*, Department of Hydrology and Water Resources, The University of Arizona, Tucson, Ariz, USA, 2014.

[2] E. Tzen and R. Morris, "Renewable energy sources for desalination," *Solar Energy*, vol. 75, no. 5, pp. 375–379, 2003.

[3] R. K. Kamali, A. Abbassi, S. A. S. Vanini, and M. S. Avval, "Thermodynamic design and parametric study of MED-TVC," *Desalination*, vol. 222, no. 1–3, pp. 596–604, 2008.

[4] R. K. Kamali and S. Mohebinia, "Experience of design and optimization of multi-effects desalination systems in Iran," *Desalination*, vol. 222, no. 1–3, pp. 639–645, 2008.

[5] M. Skiborowski, A. Mhamdi, K. Kraemer, and W. Marquardt, "Model-based structural optimization of seawater desalination plants," *Desalination*, vol. 292, pp. 30–44, 2012.

[6] B. Najafi, A. Shirazi, M. Amin Yavari, F. Rinaldi, and R. A. Taylor, "Exergetic, economic and environmental analyses and multi objective optimization of an SOFC-gas turbine hybrid cycle coupled with an MSF desalination system," *Desalination*, vol. 334, pp. 46–59, 2014.

[7] H. Shahandeh, J. Ivakpour, and N. Kasiri, "Internal and external HIDiCs (heat-integrated distillation columns) optimization by genetic algorithm," *Energy*, vol. 64, pp. 875–886, 2014.

[8] I. Janghorban Esfahani and C. K. Yoo, "Feasibility study and performance assessment for the integration of a steam-injected gas turbine and thermal desalination system," *Desalination*, vol. 332, pp. 18–32, 2014.

[9] K. Ansari, H. Sayyaadi, and M. Amidpour, "Thermoeconomic optimization of a hybrid pressurized water reactor (PWR) power plant coupled to a multi effect distillation desalination system with thermo-vapor compressor (MED-TVC)," *Energy*, vol. 35, no. 5, pp. 1981–1996, 2010.

[10] H. Sayyaadi, A. Saffari, and A. Mahmoodian, "Various approaches in optimization of multi effects distillation desalination systems using a hybrid meta-heuristic optimization tool," *Desalination*, vol. 254, no. 1–3, pp. 138–148, 2010.

[11] M. H. Khoshgoftar Manesh, H. Ghalami, M. Amidpour, and M. H. Hamedi, "Optimal coupling of site utility steam network with MED-RO desalination through total site analysis and exergoeconomic optimization," *Desalination*, vol. 316, pp. 42–52, 2013.

[12] R. Silva, M. Berenguel, M. Pérez, and A. Fernández-Garcia, "Thermo-economic design optimization of parabolic trough solar plants for industrial process heat applications with memetic algorithms," *Applied Energy*, vol. 113, pp. 603–614, 2014.

[13] S. Kalogirou, *Solar Energy Engineering: Processes and Systems*, Elsevier, New York, NY, USA, 1st edition, 2009.

[14] A. E. Kabeel and E. M. S. El-Said, "A hybrid solar desalination system of air humidification-dehumidification and water flashing evaporation. Part I. A numerical investigation," *Desalination*, vol. 320, pp. 56–72, 2013.

[15] A. E. Kabeel and E. M. S. El-Said, "A hybrid solar desalination system of air humidification, dehumidification and water flashing evaporation: part II. Experimental investigation," *Desalination*, vol. 341, pp. 50–60, 2014.

[16] Z. Chang, H. Zheng, Y. Yang, Y. Su, and Z. Duan, "Experimental investigation of a novel multi-effect solar desalination system based on humidificationdehumidification process," *Renewable Energy*, vol. 69, pp. 253–259, 2014.

[17] X. Li, G. Yuana, Z. Wanga, H. Lib, and Z. Xub, "Experimental study on a humidification and dehumidification desalination system of solar air heater with evacuated tubes," *Desalination*, vol. 351, pp. 1–8, 2014.

[18] G. Franchini and A. Perdichizzi, " Modeling of a solar driven HD (humidification-dehumidification) desalination system," *Energy Procedia*, vol. 45, pp. 588–597, 2014.

[19] O. Ansari, M. Asbik, A. Bah, A. Arbaoui, and A. Khmou, "Desalination of the brackish water using a passive solar still with a heat energy storage system," *Desalination*, vol. 324, pp. 10–20, 2013.

[20] M. Zamena, S. M. Soufaria, S. AbbasianVahdata et al., "Experimental investigation of a two-stage solar humidification-dehumidification desalination process," *Desalination*, vol. 332, no. 1, pp. 1–6, 2014.

[21] F. Nematollahi, A. Rahimi, and T. T. Gheinani, "Experimental and theoretical energy and exergy analysis for a solar desalination system," *Desalination*, vol. 317, pp. 23–31, 2013.

[22] H. Ben Bacha, "Dynamic modeling and experimental validation of a water desalination prototype by solar energy using humidification dehumidification process," *Desalination*, vol. 322, pp. 182–208, 2013.

[23] K. R. Ranjan and S. C. Kaushik, "Exergy analysis of the active solar distillation systems integrated with solar ponds," *Clean Technologies and Environmental Policy*, vol. 16, no. 5, pp. 791–805, 2014.

[24] THERMIE Program, *Desalination Guide Using Renewable Energies*, CRES, Athens, Greece, 1998.

[25] R. Z. Hu and X. Chen, "A novel integrated solar desalination system with multi-stage evaporation/heat recovery processes," *Renewable Energy*, vol. 64, pp. 26–33, 2014.

[26] Y. B. Tao and Y. L. He, "Numerical study on coupled fluid flow and heat transfer process in parabolic trough solar collector tube," *Solar Energy*, vol. 84, no. 10, pp. 1863–1872, 2010.

[27] A. Farouk Kothdiwala, B. Norton, and P. C. Eames, "The effect of variation of angle of inclination on the performance of low-concentration-ratio compound parabolic concentrating solar collectors," *Solar Energy*, vol. 55, no. 4, pp. 301–309, 1995.

[28] V. Gnielinski, "New equations for heat and mass transfer in turbulent pipe and channel flow," *International Chemical Engineering*, vol. 16, no. 2, pp. 359–363, 1976.

[29] F. Incropera and D. DeWitt, *Fundamentals of Heat and Mass Transfer*, John Wiley & Sons, New York, NY, USA, 3rd edition, 1990.

[30] M. Ouagued, A. Khellaf, and L. Loukarfi, "Estimation of the temperature, heat gain and heat loss by solar parabolic trough collector under Algerian climate using different thermal oils," *Energy Conversion and Management*, vol. 75, pp. 191–201, 2013.

[31] V. E. Dudley, G. J. Kolb, and A. R. Mahoney, "Test results: SEGS LS-2 solar collector," Tech. Rep. SAND94-1884, SANDIA National Laboratories, Albuquerque, NM, USA, 1994.

[32] Y. S. Touloukian and D. P. DeWitt, *Radiative Properties, Nonmetallic Solids*, vol. 8 of *Thermophysical Properties of Matter*, Plenum Press, New York, NY, USA, 1972.

[33] H. T. El-Dessouky, H. M. Ettouney, and F. Mandani, "Performance of parallel feed multiple effect evaporation system for seawater desalination," *Applied Thermal Engineering*, vol. 20, no. 17, pp. 1679–1706, 2000.

[34] J.-C. Han and L. S. Fletcher, "Falling film evaporation and boiling in circumferential and axial grooves on horizontal tubes," *Industrial & Engineering Chemistry Process Design and Development*, vol. 24, no. 3, pp. 570–575, 1985.

[35] L. Xu, M. Ge, S. Wang, and Y. Wang, "Heat-transfer film coefficients of falling film horizontal tube evaporators," *Desalination*, vol. 166, no. 1-3, pp. 223–230, 2004.

[36] K. Wangnick, "How incorrectly determined physical and constructional properties in the seawater and brine regimes influence the design and size of an MSF desalination plant-stimulus for further thoughts," in *Proceedings of the IDA World Congress on Desalination and Water Science*, pp. 201–218, Abu Dhabi, UAE, 1995.

[37] A. Bejan, G. Tsatsaronis, and M. Moran, *Thermal Design and Optimization*, John Wiley & Sons, New York, NY, USA, 1996.

[38] M. A. Rosen and I. Dincer, "Exergoeconomic analysis of power plants operating on various fuels," *Applied Thermal Engineering*, vol. 23, no. 6, pp. 643–658, 2003.

[39] A. Esmaieli, M. P. Keshavarz, S. E. Shakib, and M. Amidpour, "Applying different optimization approaches to achieve optimal configuration of a dual pressure heat recovery steam generator," *International Journal of Energy Research*, vol. 37, no. 12, pp. 1440–1452, 2012.

[40] S. R. Hosseini, M. Amidpour, and S. E. Shakib, "Cost optimization of a combined power and water desalination plant with exergetic, environment and reliability consideration," *Desalination*, vol. 285, pp. 123–130, 2012.

[41] A. G. Kaviri, M. N. M. Jaafar, and T. M. Lazim, "Modeling and multi-objective exergy based optimization of a combined cycle power plant using a genetic algorithm," *Energy Conversion and Management*, vol. 58, pp. 94–103, 2012.

[42] A. Baghernejad and M. Yaghoubi, "Exergoeconomic analysis and optimization of an Integrated Solar Combined Cycle System (ISCCS) using genetic algorithm," *Energy Conversion and Management*, vol. 52, no. 5, pp. 2193–2203, 2011.

[43] M. Hosseini, I. Dincer, P. Ahmadi, H. B. Avval, and M. Ziaasharhagh, "Thermodynamic modelling of an integrated solid oxide fuel cell and micro gas turbine system for desalination purposes," *International Journal of Energy Research*, vol. 37, no. 5, pp. 426–434, 2013.

[44] "Eastman Chemical Company," 2014, http://www.therminol.com/.